Numerical Analysis of Different Possible Cosmologies

PHYS3080 Cosmological Parameter Report

Ryan White
s4499039
with collaborators Marin Pjetri & Lachlan Hanrahan

June 2, Semester 1 2022

Abstract

In order to better understand the behaviour of our universe, relationships between several observables and cosmological models were analysed and discussed. The analysis in the report used Friedmann's equation as a framework for analysis of cosmological data and parameters, with several equations derived from Friedmann's equation forming a basis for much of the analysis. Simulated Type Ia supernova luminosity data (consistent with Friedmann's equation) was created, and a Markov Chain Monte Carlo implementation was used to curve-fit cosmological parameters to those unknown parameters associated with each of the 9 generated datasets. These fit density parameters agreed with the data to a high degree ($1.00 \leq \chi^2_{\text{dof}} \leq 1.04$) and even accounted for the possibility of quintessence in 4 of the 9 simulated models. The associated uncertainties in these parameters were deemed to be of an acceptable degree, and these models were compared to other cosmologies in the context of each dataset so as to further validate the fit. Limitations in the analysis were discussed, and possible improvements for future studies were suggested which would allow for more thorough analysis of possible cosmologies.

1 Introduction and Background

The dynamical nature of our universe has now been known for quite some time to an increasingly precise degree. It's evident that our universe is expanding at an accelerated rate, having first started from a Big Bang wherein the universe initially rapidly expanded from an arbitrarily small region. First derived by Alexander Friedmann, the so-called *Friedmann equation* accurately describes the behaviour of the expansion of universe for a range of cosmological parameters (which dictate the contributions to expansion of different types of energy in the universe, and are derived primarily from observational data). The rewritten form of Friedmann's equation, which is the most relevant form in the context of this report, is given as

$$H(a) = H_0 \left(\sum \Omega_x a^{-3(1+w)} \right)^{1/2} \tag{1}$$

where Ω_x represents the cosmological density parameter for the energy component x, and a represents the scalefactor of the universe (such that $a = 1$ corresponds to the present day scale proportion) [2]. The equation of state, w, depends upon which component is being considered. The possible values for the equation of state are

$$w = \begin{cases} w_0 + w_a(1-a) & \text{for } \Omega_\Lambda \\ -1/3 & \text{for } \Omega_k \\ 0 & \text{for } \Omega_m \\ 1/3 & \text{for } \Omega_r \end{cases} \tag{2}$$

In equation (2), and in the remainder of the report, Ω_Λ represents the contribution of a cosmological constant, or dark energy, on the expansion of the universe, Ω_m represents the contribution of matter (both dark matter and baryonic matter), Ω_r represents the contribution of radiation pressure, and Ω_k represents the curvature component [2], calculated as

$$\Omega_k = 1 - \Omega_m - \Omega_\Lambda - \Omega_r \tag{3}$$

Of course, there are two mystery terms for the equation of state for dark energy in equation (2); w_0 corresponds to the equation of state parameter in the present day, where w_a represents the time-varying (more specifically, *scale*-varying) equation of state.
It's worth noting that the current best accepted values for these parameters in our universe are $\Omega_m = 0.30 \pm 0.05$, $\Omega_\Lambda = 0.70 \pm 0.05$ (via the assumed flatness of our universe, which also implies $\Omega_k = 0$), $\Omega_r \approx 0$, and the dark energy equation of state has $w_0 = -1$ and $w_a = 0$ [3].

With nothing more than these parameters and equation (1), the scale of the universe versus its age can be

computed. First, note that

$$H = \frac{\dot{a}}{a} \Rightarrow \frac{da}{dt} = aH \tag{4}$$

For ease of notation, note that $da/dt = \dot{a}$, and so rearranging the Freidmann equation gives

$$\int_0^t dt = \int_0^a \frac{1}{\dot{a}}\, da \tag{5}$$

Setting the lower bounds to represent the present day values gives the lookback time of the universe, which represents the time axis in relation to the present day. Mathematically, that is

$$\int_{t_0=0}^t dt = \int_1^a \frac{1}{\dot{a}}\, da \tag{6}$$

Plotting this for a range of a values, beginning at $a = 0$ for the beginning of our universe and up to $a = 2$ (for when the universe will be double its current scale), effectively shows the expansion history of the universe.

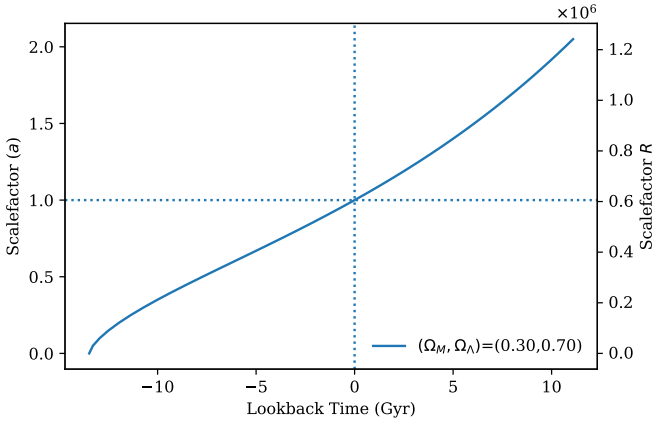

Figure. 1 With the aforementioned cosmological parameters for our universe, it's clear that the universe initially underwent a period of rapid expansion just after the Big Bang ($a = 0$). After this period, the expansion ceased acceleration up until just before the present day where the slope now has an increasing gradient.

Figure 1 begs the question of what is driving the periods of accelerated expansion. Due to the different parameter equations of state in the Friedmann equation, different parameters dominate cosmological expansion at different epochs. In general, the more negative the power that is associated with a parameter, the earlier that parameter dominates the expansion. To find the relative contribution of each parameter, its density must be divided by the total density. That is,

$$\frac{\Omega_i}{\Omega_{\text{tot}}} = \frac{\Omega_i a^{-3(1+w_i)}}{\Omega_r a^{-4} + \Omega_m a^{-3} + \Omega_\Lambda a^{-3(1+w_0+w_a(1-a))}} \tag{7}$$

where the curvature term was omitted due to the approximate flatness over almost all cosmological time. The associated epochs of parameter domination are shown in Figure 2.

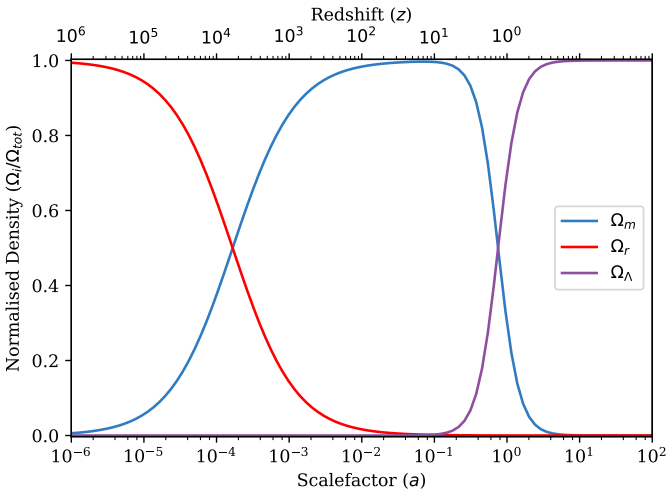

Figure. 2 Each of the three main cosmological parameters dominates at different periods in the universes evolution, shown on the x-axis with a log-scale. Since the y-axis is the relative contribution of the density, normalised to 1 (the total density), a parameter dominating expansion means that the other two must have a smaller influence.

The upper x-scale in Figure 2 shows an important relationship between distance relations in cosmology. The observed redshift of light (the wavelength change due to a doppler shift dependent on radial velocity) for distant light sources is intrinsically linked to the scale of the universe at the time of the light emission. This *cosmological redshift* is related to the scalefactor a by

$$a = \frac{1}{1+z} \quad \Longleftrightarrow \quad z = \frac{1-a}{a} \tag{8}$$

Due to the inverse nature of this relationship, observing objects at higher cosmological redshift effectively corresponds to observing them at an earlier time in the universe. This is an important tool in analysing the physics and state of the universe at different cosmological epochs, and will be of particular importance later in the report. A graphical representation of these relationships is shown in Appendix 5.2, namely in Figures 17 and 18.

The magnitude of cosmological redshift that light sources are characterised by is subject mainly to two key variables which are fundamentally linked; distance and relative velocity. Since on large scales the universe is approximately homogeneous, objects at a specific distance move in unison relative to our viewpoint. In other words, all light sources at some distance are characterised by roughly the same radial velocity relative to Earth. This distance-velocity relationship is given by the Hubble constant, $H_0 \approx 70$ km/s/Mpc [1], which approximates the radial velocity of an object in terms of its distance. Since the universe is expanding and its scalefactor constantly changing, the Hubble constant is

no constant at all, and is decreasing at a well defined rate.

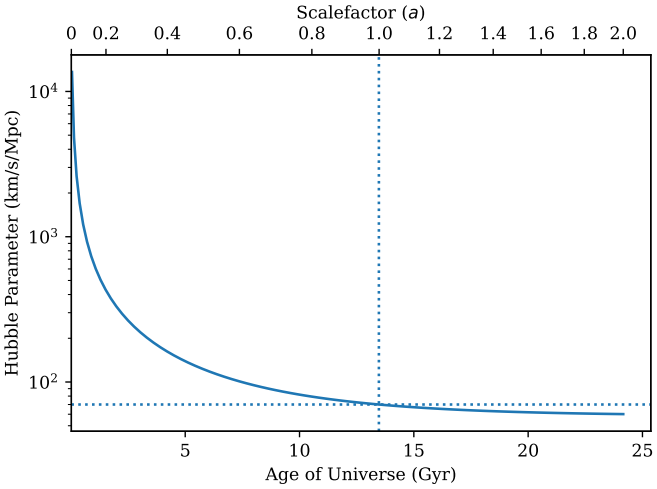

Figure. 3 The Hubble Parameter over time for our universe, with the density parameters detailed earlier. Horizontal and vertical lines were plotted such that their intersection aligns to the present-day Hubble value, H_0 and $a = 1$. Although the Hubble parameter is decreasing (perhaps contrary to intuition), the universe is expanding at an accelerating rate. One way of rationalising this is that the change in distance between objects is cumulative, and so even though the Hubble Parameter is decreasing, the distance between objects is increasing faster and so the relative radial velocity increases accordingly (corresponding to an accelerated expansion).

The equation that describes the Hubble parameter over time (more specifically, scalefactor) is exactly the Friedmann equation.
One of the more fundamental tools in cosmology is being able to use Friedmann's equation in terms of redshift to determine the Hubble parameter and other variables;

$$H(z) = H_0 \left(\sum \Omega_i (1+z)^{3(1+w_i)} \right)^{1/2} \tag{9}$$

The importance of this is that the redshift of a light source is an observable, rather than scalefactor which is not. As such, several fundamental details of the universe can be inferred just from seeing by how much emission and absorption lines in spectra have shifted.
Given that light has a finite velocity, the light that reaches an observer on Earth has been travelling for some time, and since the universe is expanding at a rate specified by equation (9), the light has actually been travelling farther than it would have in a static universe. In fact, at sufficiently high redshift ($z \gtrsim 1.5$), light was emitted from a source at a smaller proper distance from Earth than that of a source at a slightly lower redshift. This relationship between light emission distance and redshift is shown in Figure 4.

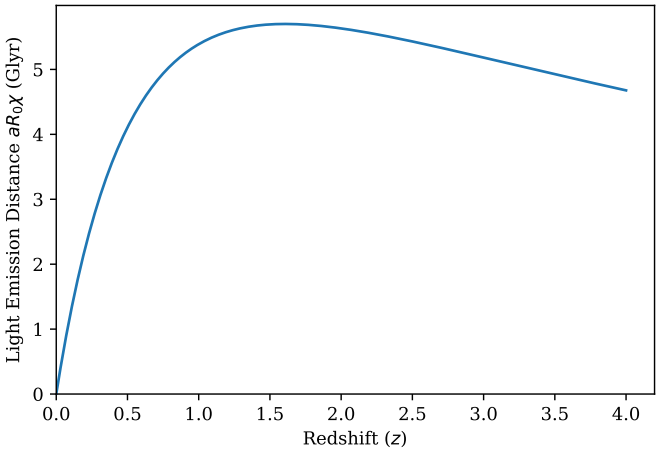

Figure. 4 Due to the expanding universe, light at a sufficiently high redshift was emitted at a closer distance to Earth than that at a slightly lower redshift. This is primarily because the space between Earth and the light source had expanded by such an extent *while* the light was travelling, that it had to traverse a much larger distance and hence arrive at an observer at a later time.

The emission distance is calculated in terms of the comoving distance via

$$d_{\text{emit}} = aR_0\chi = ac \int_a^1 \frac{1}{a\dot{a}}\, da = \frac{c}{1+z} \int_0^z \frac{1}{H(z)}\, dz \tag{10}$$

where the comoving distance is simply

$$R_0\chi = c \int_0^z \frac{1}{H(z)}\, dz \tag{11}$$

and the term R_0 in the above equations is the present-day radius of curvature (in units of distance). Multiplying the comoving distance by this radius of curvature yields physically realisable distance results with appropriate units. The relationship between comoving distance and redshift is shown in Figure 19, which may help to interpret Figure 5.
Since the universe is expanding at an accelerated rate, there will be a point where some objects that we can currently observe (from light emitted in the past) can no longer be observed. All events on the spacetime diagram shown in Figure 5 that lie outside of the event horizon will never be seen by an observer with Earth's spatial coordinates. The equation to calculate the event horizon is effectively a rearranged form of equation (11), with different bounds and in terms of scalefactor:

$$R_0\chi = c \int_a^\infty \frac{1}{a\dot{a}}\, da = c \int_a^\infty \frac{1}{a^2 H(a)}\, da \tag{12}$$

The bounds of the integral in equation (12) represents the distance that light can travel between the current scale factor, a, and the "end" of the universe, as $t \to \infty$. All events within the Event Horizon may eventually be

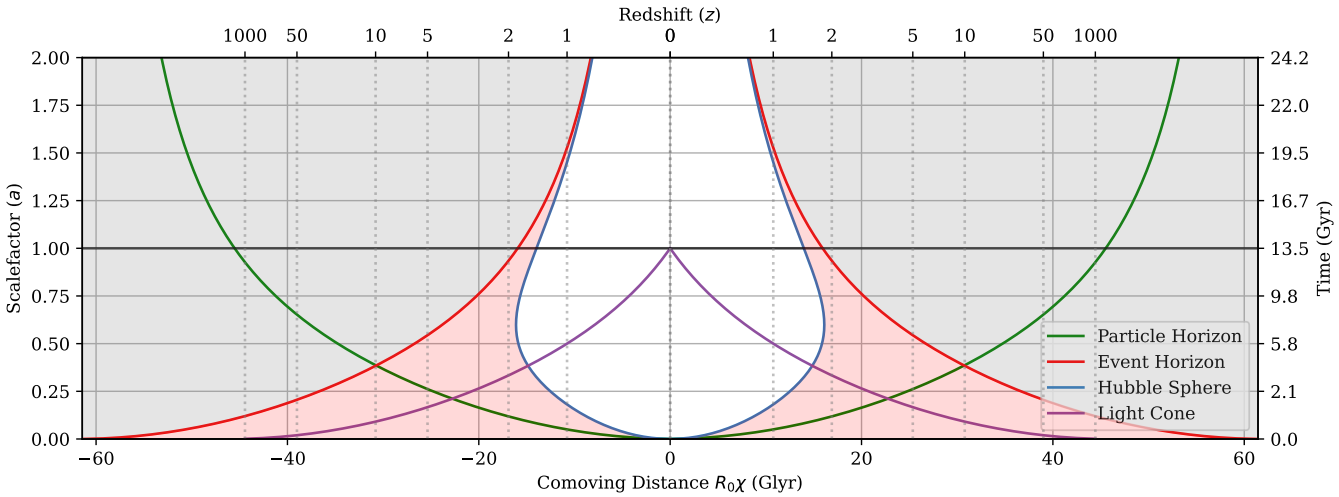

Figure. 5 Spacetime diagram for our universe with $(\Omega_m, \Omega_\Lambda) = (0.3, 0.7)$. Due to the expanding nature of the universe, all horizons are represented by curved geodesics. Between $a = 0$ and $a = 1$, the particle horizon effectively mirrors the observers light cone which is a physical property of the relationship between the two. Clearly, as $t \to \infty$, the event horizon begins to converge to a (relatively) small comoving distance from the observer, showing that the set of all possible causal interactions increases at a decreasing rate until eventually no interaction is possible. As the universe is expanding at an accelerating rate in the present and future times, the Hubble sphere is 'shrinking' and is effectively approaching the observer at $R_0\chi = 0$.

observed by an observer on Earth, but only those within our light cone may be observed in the present day. The events within the bounds of the light cone have causal influence on events at our spatial coordinates in that they may interact with us from the light they emit. The extent of the light cone is calculated via equation (12) with integral bounds of $a = a \to 1$.

The furthest distance for which we can currently observe events is given by the particle horizon (where the extent of the particle horizon signifies the current comoving distance to the earliest events within our light cone). Once again, the extent of the particle horizon is given by equation (12) with bounds of $a = 0 \to a$.

The final aspect of Figure 5 is the Hubble distance (or equivalently, radius), which corresponds to the sphere where the recession velocity of light sources is the speed of light, $v_{\text{rec}} = c$. That is, the comoving Hubble radius is

$$r_\chi = \frac{c}{aH(a)} = \frac{c}{\dot{a}} \tag{13}$$

All discussion up to this point has been in the context of our universe, with $(\Omega_m, \Omega_\Lambda) = (0.3, 0.7)$, but to fully appreciate the versatility of Friedmann's equation and further validate our own derived cosmological parameters, other possible universes must be examined.

An important characteristic of a universe is its age. As shown in the multitude of graphs above, our universe has an age (as predicted by Friedmann's equation) of about 13.5 billion years, but for other universes this number is heavily dependent on the cosmological parameters which characterise that universe. Figure 6 shows a surface plot of universe age with respect to the parameters which define that universe.

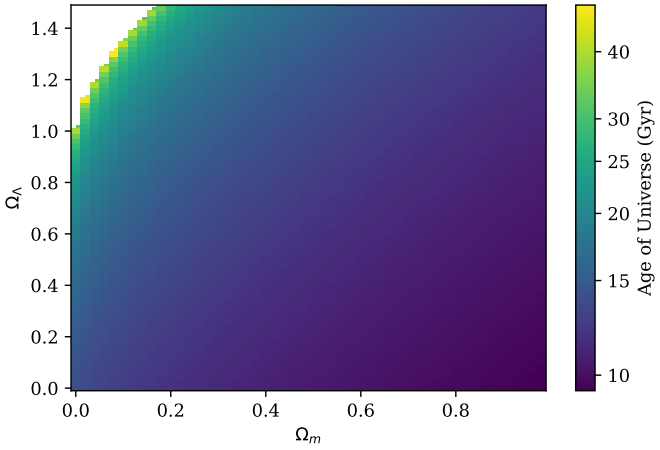

Figure. 6 The age of the universe (Gyr) with respect to the parameters which define said universe. For sufficiently low matter density and correspondingly high dark energy density, the age of the universe will approach infinity, and consequently no Big Bang would have been predicted from Friedmann's equation. A similar, albeit less extreme, example of this is seen in Figure 7 for the curve defined by $(\Omega_m, \Omega_\Lambda) = (0, 0.7)$. A contextually similar plot is shown in Figure 20 in the Appendices, which alters one parameter with the other fixed (which effectively corresponds to a horizontal and vertical line overlaid onto this plot).

The age of a universe can be found by setting the upper integral bound in equation (5) to $a = 1$, although

this isn't a 'catch-all' case as some cosmologies will correspond to the integral being divergent. Such examples of this are shown in Figure 6 in the upper left corner where universes will have no Big Bang. In fact, a condition arises as to whether or not a universe could have had a Big Bang. For some Ω_m and Ω_Λ, this condition for a universe to have no Big Bang is

$$\Omega_\Lambda \geq 4\Omega_m \left(\text{coss}\left[\frac{1}{3}\text{coss}^{-1}\left(\frac{1-\Omega_m}{\Omega_m}\right)\right]\right)^3 \qquad (14)$$

where $\text{coss}(x)$ is defined as $\cosh(x)$ when $\Omega_m \leq 1/2$ and $\cos(x)$ when $\Omega_m > 1/2$.

The cosmological parameters influence not only the age of a universe, but its expansion history too. To help illustrate this, Figure 7 shows the expansion history for universes with fixed dark energy density and varying matter density.

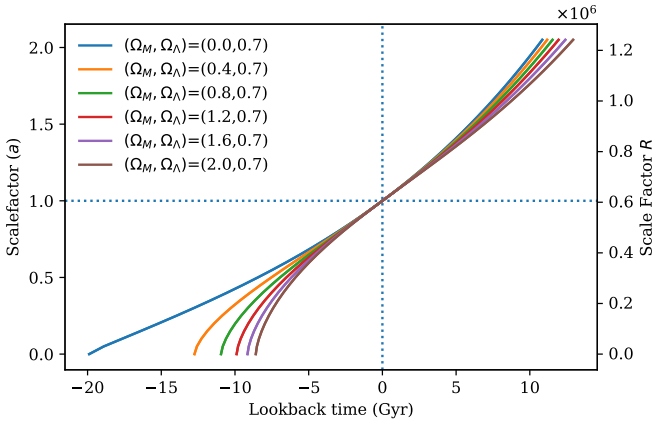

Figure. 7 The expansion history for varying matter densities (with fixed Ω_Λ) correlate with younger universes characterised by steeper expansion in order to meet a present day value of $H_0 \approx 70$ km/s/Mpc.

Non-zero matter density thus correlates with an initial inflationary period followed by gradual deceleration as the matter density dominates. When the dark energy begins to dominate close to the present epoch, all universes begin accelerating in their expansion.
Clearly, the expansion history of a universe is heavily dependent on the cosmological parameters which define it. Even small changes in density parameters extrapolate to significant differences in expansion over large timescales. These changes directly affect the observable characteristics of distant light sources and how they appear to an observer at our spacetime coordinates.

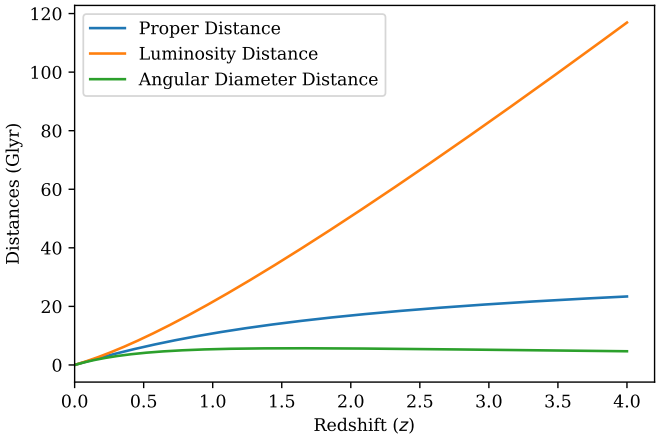

Figure. 8 This comparison between comoving distance, luminosity distance, and angular diameter distance for our universe show how the expansion history affects how distant objects appear. Since proper distance is defined as the comoving distance in the present day, this is the baseline for which distance measures should be compared. Since the universe is expanding at an accelerated rate, the inferred distance as calculated from the luminosity of a light source increases sharply with redshift due to the loss of energy in photons and the inverse square law. The photons observed from a source have travelled proportionally farther due to expansion, and so the object appears further away than it really is. In contrast to the luminosity distance, the angular diameter distance decreases after a redshift threshold so that distant objects actually appear closer. This is due, once again, to the expansion of the universe. When the light was emitted by these distant sources, the universe was much smaller and so the source was closer to the observer. The angular diameter of the object is preserved across expansion (after light emission), and the object appears larger than it should be in the sky, directly corresponding to the inferred distance from angular-diameter measures being smaller than it actually should be. An incredibly intuitive visualisation of this is shown in [4].

The main observable in the context of data analysis is luminosity, and so the luminosity distance, D_L, is the most readily-calculable value of the three distance measures. Directly related to this is the magnitude of the light source, where the apparent magnitude observed is given by

$$m(\mathcal{P}, z) = 5\log_{10}(D_L(\mathcal{P}, z)) + 25 + M \qquad (15)$$

where $\mathcal{P}$ is the set of cosmological parameters, and M is the inferred absolute magnitude of some light source. What is of more relevance in the context of curve-fitting data in order to determine the cosmological parameters in a universe is the distant modulus, defined by

$$\mu(\mathcal{P}, z) = 5\log_{10}(D_L(\mathcal{P}, z)) + 25 = m(\mathcal{P}, z) - M \qquad (16)$$

In fact, the luminosity distance for some redshift can be calculated using the comoving distance [equation (11)], by

$$D_L = R_0 S_k(\chi)(1+z) \tag{17}$$

where the function S_k is a curvature correction which takes on the values

$$S_k(\chi) = \begin{cases} \sinh(\chi) & \Omega_k > 0 \\ \chi & \Omega_k = 0 \\ \sin(\chi) & \Omega_k < 0 \end{cases} \tag{18}$$

And so given some light source magnitudes and redshifts, the cosmological parameters of a universe can be found such that the distance modulus model best fits the data. In order to simplify further, note that

$$R_0 = \frac{c}{H_0\sqrt{|\Omega_k|}}$$

and so equation (17) can be rephrased as

$$D_L = \frac{c}{H_0\sqrt{|\Omega_k|}} S_k(\chi)(1+z) = \frac{c}{H_0} D'_L \tag{19}$$

and consequently, due to a multiplicative log law, equation (16) becomes

$$\mu(\mathcal{P},\, z) = 5\log_{10}(D'_L(\mathcal{P},\, z)) + 5\log_{10}(c/H_0) + 25$$

In this report, simulated supernova data will be used as the light source for which the cosmological parameters will be determined. In the real world, the intrinsic luminosity of Type Ia supernovae aren't known to an arbitrary level of precision and so there is some inherent uncertainty in the M value present in equations (15) and (16), ΔM. Similarly, there is also a non-negligible error in the value of Hubble's constant, H_0. Define $\mathcal{M} \coloneqq 5\log_{10}(c/H_0) + 25 + \Delta M$ for which the distance modulus can be marginalized over. Equation (16) then finally becomes

$$\mu(\mathcal{P},\, z) = 5\log_{10}(D'_L(\mathcal{P},\, z)) + \mathcal{M} \tag{20}$$

and is the equation for which a model can be compared to data in order to achieve the 'best fit' cosmological parameters.

2 Methods and Results

In order to investigate how varying cosmological parameters impacts the expansion history and characteristics of a universe, multiple simulated supernova data sets were produced according to the methodology in section 2.1. Throughout the generation and analysis, the programming language Python was used extensively. Notable packages utilised included, but was not limited to, `numpy`, `matplotlib`, `emcee`, `corner`, `scipy`, and `multiprocessing`.

2.1 Simulated Data Generation

To begin with, 9 datasets were produced according to the following criteria:

- Data00 consists of data aligning perfectly to theory, with $(\Omega_m,\, \Omega_\Lambda) = (0.3,\, 0.7)$ and no random scatter about the model.
- Data0 is similar to Data00, but with random scatter about the model.
- Datasets 1 to 3 are characterised by a model with uncertain matter and dark energy densities, but all other parameters are fixed, with $(\Omega_r,\, w_0,\, w_a) = (0,\, -1,\, 0)$.
- Datasets 4 to 7 potentially have any and/or all parameters varied from those of our universe.

The purpose of this dataset hierarchy was to progressively test more complicated models against the available tools. Arguably the most important dataset is Data00, which acted as a sort of benchmark dataset in order to calibrate the model; if the curvefitting could output the correct parameters for Data00, then the method for which the model was obtained is sound.

As to how the data was actually generated, all of the relevant theory has been introduced already. Approximately 200 redshift data points were generated between $z = 0$ and $z = 1$, where data points with $z \leq 0.02$ were omitted. These were omitted as the relative error in magnitudes for supernovae at this redshift would be too high to reliably fit a model to. In real world contexts, fitting data at such low redshifts becomes problematic due to the contributions of peculiar redshifts, z_p, which is the result of radial velocity from factors other than cosmological expansion (such as gravitational attraction).
The theoretical magnitude at each redshift was calculated according to equation (15), with some vertical scatter applied according to a standard normal distribution (centered at 0 with standard deviation of 1).

The distance modulus equation of course requires some cosmological parameters in order to decide at which magnitude a redshift point belongs at. This task was handed to an all-wise supervisor of the author and contributors, who chose parameters seemingly at random according to the prior distributions in Table 1.

With all of the data generated, the task of finding the corresponding parameters for each dataset was at hand.

2.2 Parameter Fitting

As detailed earlier, all data analysis was performed in Python using the aforementioned packages. With this,

Parameter	Prior
Ω_m	[0, 1]
Ω_Λ	[0, 1]
Ω_r	[0, 1]
w_0	[−2, 0]
w_a	[−1.5, 0.5]

Table 1 The prior distributions shown above are only truthfully applicable to datasets 4 to 7, where any arrangement of parameters could be varied. For datasets 1-3, only Ω_m and Ω_Λ were subject to the distributions above, with $(\Omega_r, w_0, w_a) = (0, -1, 0)$.

three main parameter fitting methods were attempted: Nested Grid Search, a method of Successive Approximation, and Markov Chain Monte Carlo. Each approach was tested with a fully functioning code structure, although to varying results which will be covered in the respective subsections.

2.2.1 Nested Grid Search

The first method attempted was a simple, although computationally inefficient nested grid search. The process of this was to evenly distribute points around n-dimensional parameter space, and then assess the fit of the associated parameters according to the relevant data. The computational inefficiency arose from the *nested* aspect of the grid search, where for loops were placed within each other in order to search across all possible combinations of parameters.
This approach worked well in a suitable duration for datasets 00 to 3, where the parameter space was only 2-dimensional. An example fit is shown in Figure 9.

The most-likely fit was determined based on minimising the χ^2 value, which is a statistical measure of correlation calculated by

$$\chi^2 = \sum_i \left(\frac{\mu_{\text{model}} - \mu_i}{\sigma_i} \right)^2 \tag{21}$$

such that the best possible fit of a model to data results in $\chi^2 = 0$.

Unfortunately, for the more complicated datasets 4 to 7 that necessitated parameter searching in 5-dimensional parameter space, the computation time because too long even with multiprocessing (sharing CPU load across multiple cores). Two solutions were immediately apparent: either reduce grid resolution or use a different model. Since a lower resolution would correspond to parameters potentially significantly deviating from their true values, different methods of model fitting were necessary.

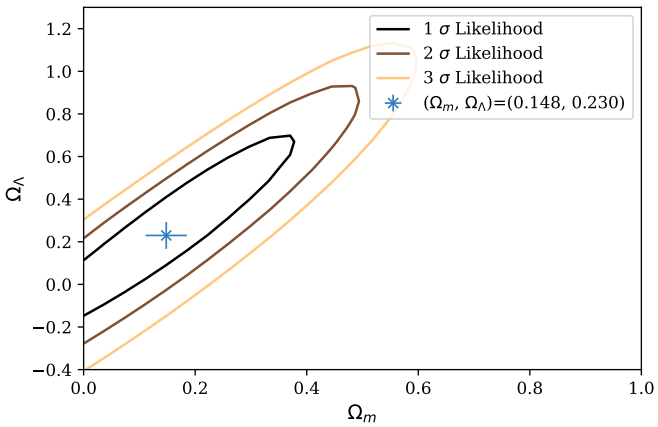

Figure. 9 The parameter space best-fit is shown with 1, 2, and 3 standard deviation contours overlaid for the fit to Data0. Exact uncertainty in best fit is given by the lines protruding from the central point, which also indicates the step size in the parameters observed. The output best fit is shown in the figure legend, $(\Omega_m, \Omega_\Lambda) = (0.148, 0.230)$. Uncertainties in this value were not calculated due to this method of search being later abandoned.

2.2.2 Method of Successive Approximation

The theory that constitutes this method is largely the same as with the nested grid search. The key distinction between them is that with a method of successive approximation, an initial low resolution grid is used wherein rough values for the best-fit parameters are obtained. The program then searches again using a smaller grid centered about the previous best fit parameters with a correspondingly lower domain. With enough steps, this method in principle can "zoom" into an arbitrarily precise set of parameters which perfectly matches the model.

Unfortunately, this method is not without its constraints. With a low resolution initial grid, the parameter search often converges onto a local minimum in the space of χ^2 values, and ends on a relatively bad fit. The solution to this is to increase the resolution of the initial grid, but to use a sufficiently high resolution grid such that the global χ^2 minimum could be found would bring with it the drawbacks associated with the primitive nested grid search method. A more precise and computationally cheap method was required.

2.2.3 Markov Chain Monte Carlo

The basic idea of the Markov Chain Monte Carlo method for curve-fitting is reasonably simple: random walkers move about an n-dimensional parameter space, progressively finding the likelihood distribution for a given set of parameters that best fits the data. The walkers can move around parameter space subject to the priors given in Table 1, and over enough iterations,

Dataset	Fitted Parameters						Age of Universe
	Ω_m	Ω_Λ	Ω_r	w_0	w_a	χ^2_{dof}	(Gyr)
Data00	$0.29^{+0.06}_{-0.07}$	$0.68^{+0.13}_{-0.15}$	0	-1	0	0.00	13.47
Data0	$0.19^{+0.12}_{-0.10}$	$0.32^{+0.24}_{-0.19}$	0	-1	0	1.00	12.93
Data1	$0.25^{+0.11}_{-0.10}$	$0.22^{+0.22}_{-0.15}$	0	-1	0	1.01	12.13
Data2	0.59 ± 0.10	$0.15^{+0.18}_{-0.11}$	0	-1	0	1.04	10.51
Data3	$0.11^{+0.11}_{-0.08}$	$0.51^{+0.20}_{-0.16}$	0	-1	0	1.01	14.58
Data4	$0.39^{+0.30}_{-0.27}$	$0.31^{+0.34}_{-0.21}$	$0.20^{+0.14}_{-0.13}$	$-0.77^{+0.46}_{-0.71}$	$-0.52^{+0.68}_{-0.66}$	1.01	9.35
Data5	0.49 ± 0.34	$0.26^{+0.41}_{-0.19}$	0.50 ± 0.18	$-0.46^{+0.34}_{-0.79}$	-0.51 ± 0.66	1.04	7.85
Data6	$0.12^{+0.12}_{-0.08}$	$0.61^{+0.23}_{-0.18}$	$0.05^{+0.05}_{-0.04}$	$-1.20^{+0.34}_{-0.45}$	$-0.64^{+0.70}_{-0.59}$	1.04	12.53
Data7	$0.09^{+0.11}_{-0.07}$	$0.48^{+0.30}_{-0.21}$	$0.04^{+0.05}_{-0.03}$	$-0.93^{+0.36}_{-0.58}$	$-0.75^{+0.71}_{-0.53}$	1.03	12.91

Table 2 Fit parameters with a non-zero uncertainty represent those fitted by the MCMC parameter optimization implementation using the prior distributions shown in Table 1, and MCMC details detailed in the main body. For each dataset, the age of the corresponding universe was calculated via setting the integral upper bound in equation (5) to $a = 1$ and substituting the curve-fit parameters for that universe into Friedmann's equation. The values in the table above represent the mean of the respective posterior distributions. The maximum-likelihood values for each dataset are given in Table 3.

eventually converge to an accurate fit to the data.

Due to the relative simplicity in searching over a 2-dimensional parameter space for datasets 00 to 3, only 10^3 iterations were needed for the walkers to converge to a reproducible posterior distribution (the distribution of likely parameter values). For the more complicated datasets 4 to 7 with a 5-dimensional parameter space, 3×10^4 iterations were used to converge to a reproducible posterior distribution. In all cases, 50 random walkers were utilised. A graphical example of *how* the walkers converged to a best-fit solution is shown in the .gif within this link.

As to the how of the implementation of MCMC, the Python `emcee` package allowed for a quick and relatively simple programming exercise. All of the code for which the project analysis was built on is available on the project's GitHub repository.

The mean of the posterior distributions for each parameter for each dataset is shown in Table 2. The "goodness of fit" quantifier is given by the reduced χ^2 value, χ^2_{dof}, calculated by

$$\chi^2_{\text{dof}} = \frac{\chi^2}{n_{\text{data}} - 1 - n_{\text{params}}} \tag{22}$$

where n_{data} is the number of data points, and n_{params} is the number of parameters being optimized. A χ^2_{dof} close to 1 represents the best possible fit, where values significantly above 1 suggest that the model is not a good fit to the data while values significantly below 1 suggest that the model is overfitting the data (for example the errorbars are too large, or there are too many parameters being fit).

Although the posterior means are the 'main' result (and are what is used as *the* best-fit parameters to plot the models against the data), it is customary to quote the maximum likelihood values for the posterior distributions also. These values are available in Table 3.

Dataset	Fitted Parameters				
	Ω_m	Ω_Λ	Ω_r	w_0	w_a
Data00	0.28	0.69	0	-1	0
Data0	0.12	0.25	0	-1	0
Data1	0.24	0.05	0	-1	0
Data2	0.59	0.00	0	-1	0
Data3	0.00	0.41	0	-1	0
Data4	0.15	0.15	0.14	-0.60	-0.80
Data5	0.15	0.00	0.40	-0.10	-0.40
Data6	0.00	0.47	0.00	-1.06	-1.50
Data7	0.00	0.30	0.00	-0.80	-1.50

Table 3 The maximum likelihood values of the posterior distributions of each parameter of each dataset. Values are quoted with no uncertainty due to the nature of the value; there may only be one global maximum associated with a distribution.

An example corner plot for a two parameter fit is shown in Figure 10, which displays the posterior distributions and the likelihood contour for the Data0 dataset (that most similar to typical data obtained in our universe).

The actual fit of this model to the Data0 data is shown in Figure 11, and aligns extremely well (with the χ^2 shown in Table 2).

Given the vast range in magnitudes shown in Figure 11,

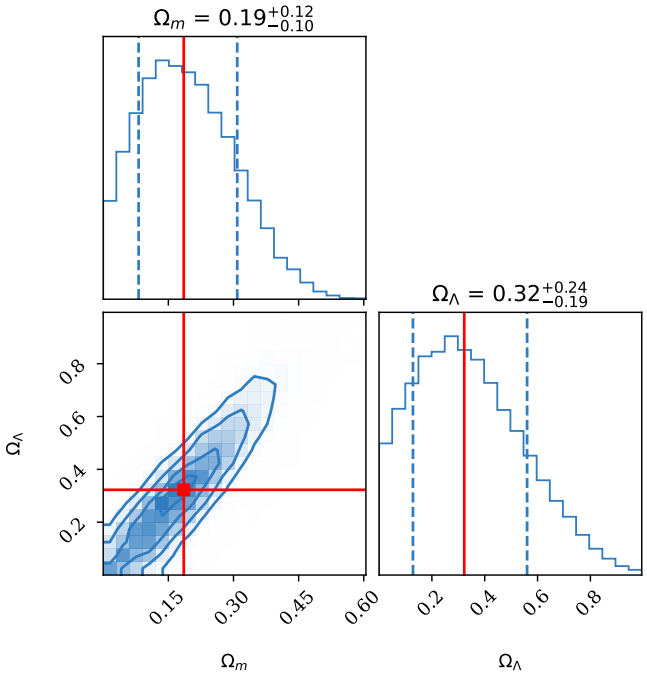

Figure. 10 Posterior distributions for each parameter fit in Data0 are shown above and to the right of the likelihood contour plot shown in the bottom left corner. The contour lines represent the 1, 2, and 3 standard deviation contours, and a deeper blue colour within the contour corresponds to an increasing likelihood of that parameter. The vertical red lines are situated at the mean of the posterior distributions, and are overlaid onto the contour with a point representing the 'best-fit' parameter coordinates. Standard deviation lines are given in the posterior distributions and are at asymmetrical intervals due to the truncated distributions as a result of the sharp prior distribution cutoff at $\Omega_i = 0$.

it can be difficult to see just how well the data fits. In order to better visualise this, the data was normalized against an "empty" universe (one with the density parameters being 0, and no time varying dark energy contribution). This was done by simply subtracting the modelled magnitude curve of the empty universe from that of the datasets. This normalized magnitude plot is shown in Figure 12.

In our universe, it is known to reasonably high precision that the matter (both baryonic and dark matter) contributes about $\Omega_m = 0.30 \pm 0.05$ to the total energy density (from galaxy cluster dynamics and baryon density oscillation data) [3]. Due to the versatility of MCMC as a method of curve-fitting, it was very easy to alter likelihood function to account for this (so that values of $\Omega_m \simeq 0.30$ were preferred). When this was done, the program fit a value of $\Omega_\Lambda = 0.50 \pm 0.13$ which, although not in perfect agreement with the agreed real-world values, fit the simulated data quite

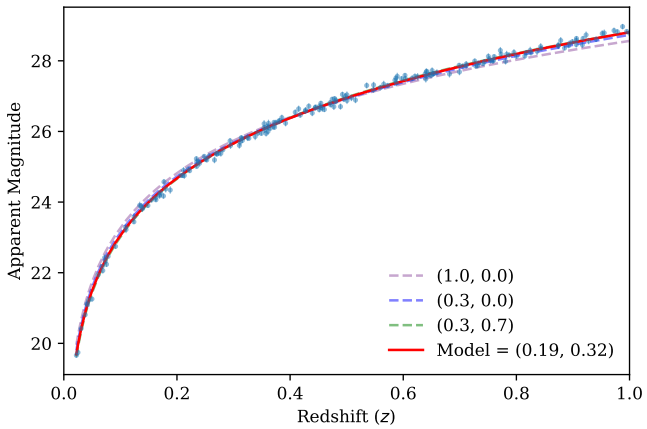

Figure. 11 The data for the Data0 set clearly follows a logarithmic curve (as predetermined in the generation), with some scatter about an implied line of best fit. The best-fit model derived from the MCMC implementation is overlaid in red, where other possible cosmologies are overlaid with a lower opacity. This was done to help show the effect of changing parameters with respect to this dataset, and serves to further validate the fit of the best-fit model.

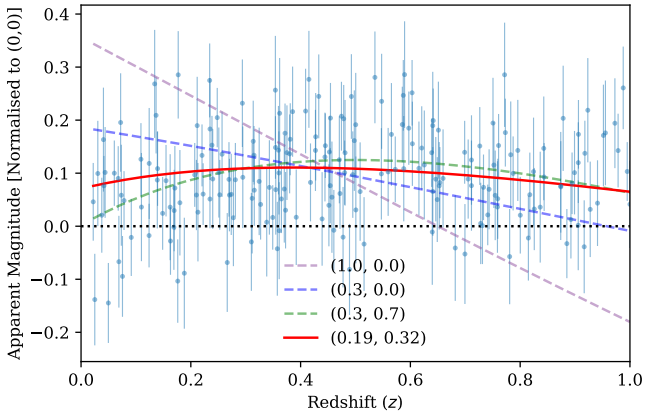

Figure. 12 The normalized magnitude plot (with respect to an empty universe) clearly magnifies the effect of the error bars in Data0, and allows for a more critical evaluation of the best-fit model. Although the data is fundamentally the same as in Figure 11, any shortfalls of the model are more readily apparent. An interesting note about this particular dataset is that the green overlay corresponding to $(\Omega_m, \Omega_\Lambda) = (0.3, 0.7)$ is the 'correct' fit for this data, since Data0 was intended to be analogous to data from our own universe. Due to the large scatter in the data, however, the best-fit parameters are different to the generation parameters, which results in a differently shaped model fit.

well with a $\chi^2_{\text{dof}} = 1.02$.
Similarly, when input a prior of flatness (assuming no radiation density, this corresponds to $\Omega_m + \Omega_\Lambda = 1.00 \pm 0.05$), a similarly accurate value was produced. The resultant posterior distribution resembled that of a Gaussian, with precise error bars corresponding to that of the flatness prior. The corner plot of this assumed flat Data0 dataset is shown in Figure 13.

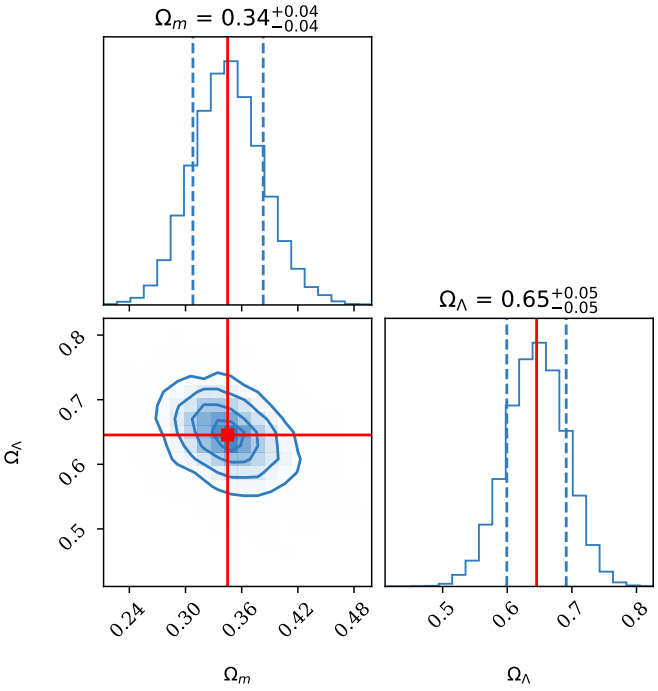

Figure. 13 When assuming a prior of flatness in the universe ($\Omega_k = 0$) for Data0, the contour of the posterior distribution is much more centrally distributed when in comparison to Figure 10. The resultant posterior distributions are almost perfect Gaussians, and the error bars are correspondingly low and symmetrical.

Since the datasets 4 to 7 varied significantly in parameter space from those of the first 5 datasets, the distributions and resultant corner plots were subject to dramatic change too. Figure 15 shows the posterior distributions of the fit parameters, with the corresponding likelihood contour plots. Figure 14 shows the fit of the corresponding mean values to the Data6 dataset.

All of the corner plots and model fit plots for the other simulated universes are available on the project's GitHub repository (linked earlier, and in the Appendices).

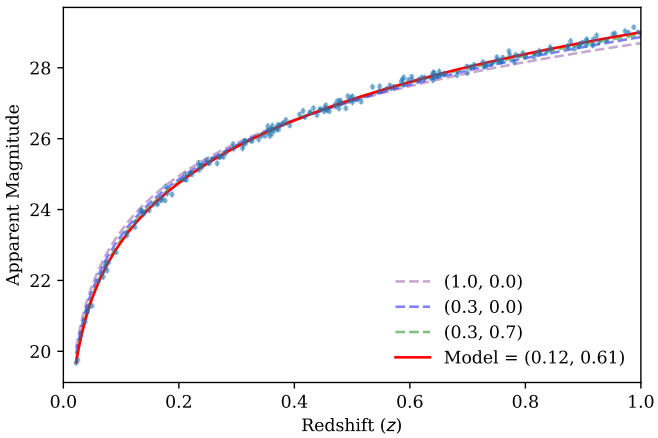

(a) The features of this graph are largely the same as in Figure 11, but with Data6 being characterised by a steeper magnitude vs redshift slope.

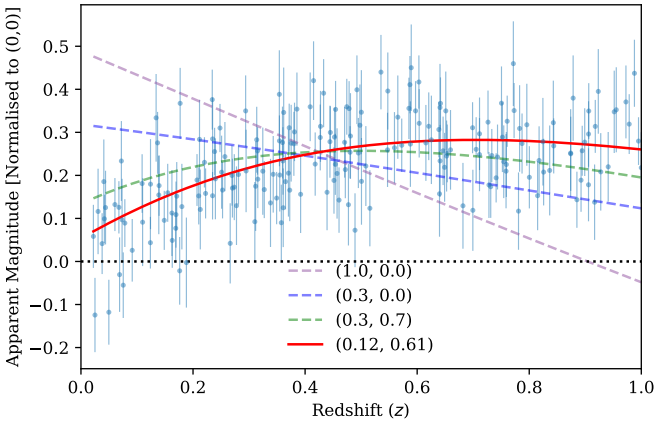

(b) As in the normalized magnitude plot for Data0, sample model fits are overlaid onto the Data6 data with the best-fit model derived from MCMC shown in red.

Figure. 14 As shown in the main results table (2), the MCMC fit for the Data6 dataset fits extremely well with a $\chi^2_{\text{dof}} = 1.04$. This dataset is characterised by a time varying dark energy contribution, which results in the exaggerated curve of the data and consequently the model.

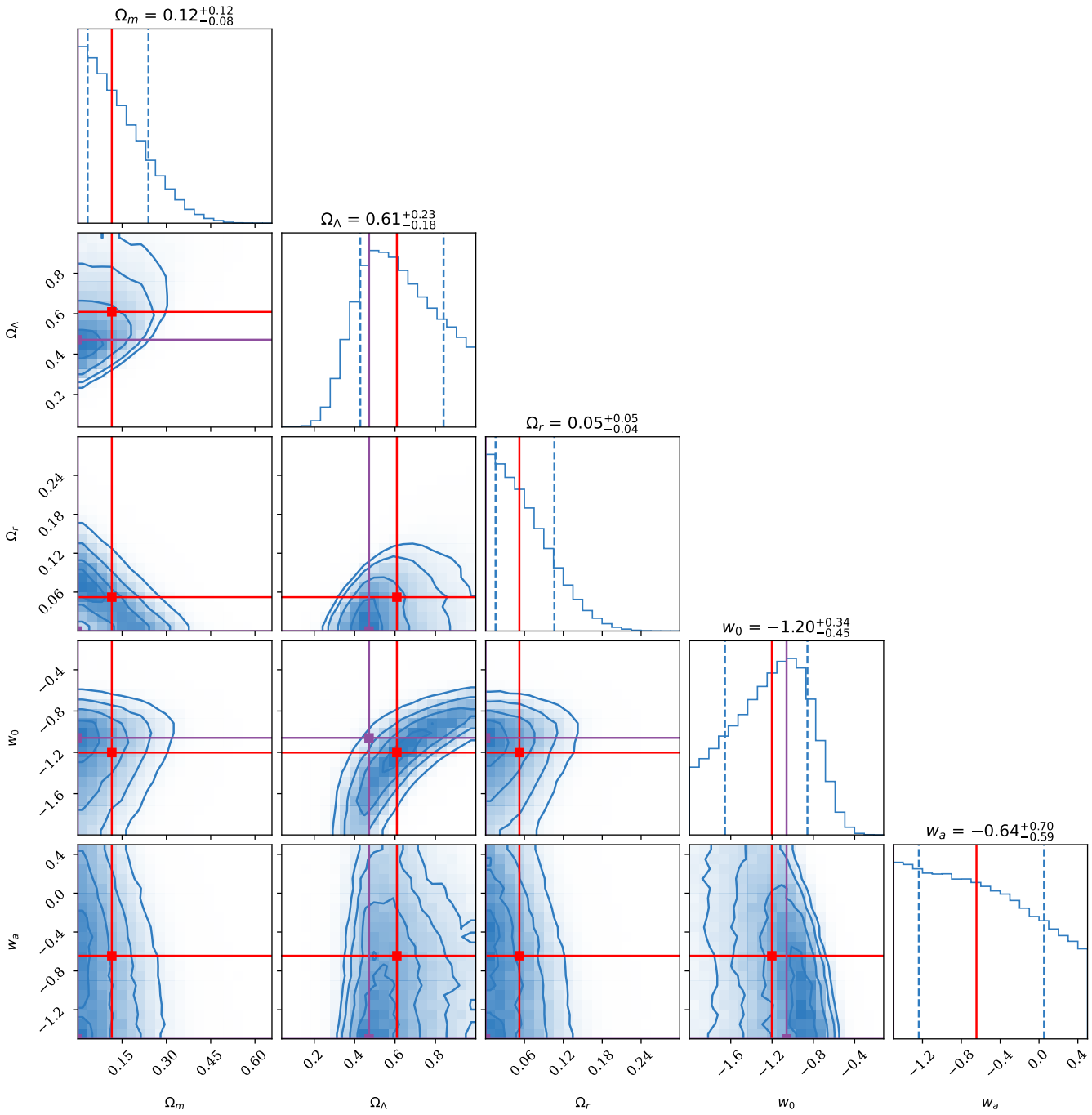

Figure. 15 The contour plot for the Data6 dataset shows fundamentally the same features as that in Figure 10, with only two main differences. Obviously, this corner plot represents the posterior distributions of 5 parameters as opposed to only two. Secondly, purple lines were overlaid corresponding to the position of the maximum likelihood value in the posterior distributions. This was done as the plot is intrinsically harder to interpret in comparison with the earlier corner plot, and so the max-likelihood lines give another aid in interpreting the contours in relation to the distributions.

3 Discussion

With all of the data collected and models fit, it's now possible to discuss the cosmologies of the different generated universes. With all of the best-fit values obtained, it is easy to plot the expansion history of each universe much in the same way as in Figure 7. This is shown in Figure 16.

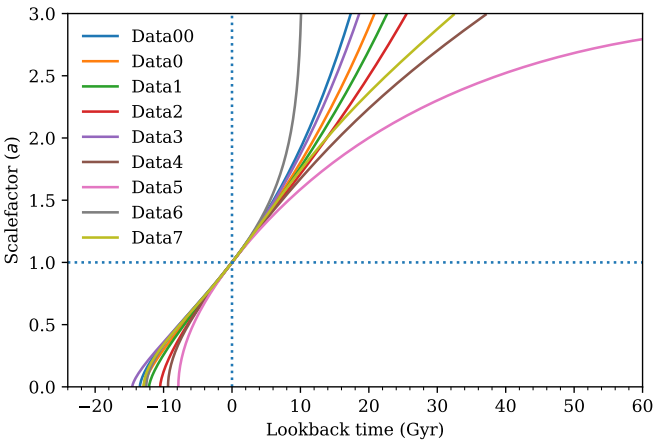

Figure. 16 The expansion history of each of the cosmologies as detailed in Table 2, where colour was chosen in order for the lines to be suitably distinct from each other.

Since all of the universes had an assumed Hubble constant of $H_0 \approx 70$ km/s/Mpc, the expansion history diagram behaves much in the same way as Figure 7. As such, they all converge to the same slope in Figure 16 at $(t, a) = (0, 1)$. A possible improvement for future studies is immediately apparent: vary the value of Hubble's constant across different universes as another extension to the model fitting.

An exciting aspect of Figure 16 that is not present in Figure 7 is the presence of a seemingly contracting universe. The main difference between fit of Data5 (which is apparently collapsing) and the others is that it is characterised by parameters which imply a closed universe, i.e. that with positive curvature ($\Omega_k < 0$). The condition for flatness in a universe is that

$$\Omega_m + \Omega_\Lambda + \Omega_r + \Omega_k = 1 \tag{23}$$

And so a universe is only flat when $\Omega_k = 0$ (according to equation (3), corresponding to constant expansion but at a decreasing rate. For $\Omega_k < 0$, a universe is closed and so gravity eventually necessitates that contraction will occur instead of constant expansion. In these cases, a universe recollapses, possibly back to an infinitesimal point provided that quintessence (time-varying dark energy) doesn't negate the contraction. For $\Omega_k > 0$, a universe is open and will expand forever at an increasing rate. For all of the generated universes, the curvature density is shown in Table 4.

Dataset	Ω_k
Data00	$0.03^{+0.14}_{-0.16}$
Data0	$0.49^{+0.27}_{-0.21}$
Data1	$0.53^{+0.25}_{-0.18}$
Data2	$0.26^{+0.21}_{-0.15}$
Data3	$0.38^{+0.23}_{-0.18}$
Data4	$0.10^{+0.47}_{-0.37}$
Data5	$-0.25^{+0.56}_{-0.43}$
Data6	$0.22^{+0.26}_{-0.20}$
Data7	$0.39^{+0.32}_{-0.22}$

Table 4 Curvature density parameters were manually calculated according to equation (3). Errors were manually propagated according to error propagation laws. As expected from the behaviour in Figure 16, Data5 is the only dataset with positive curvature.

Due to the quintessence associated with Data5, calculating the time until total recollapse is outside of the scope of this report due to the level of mathematics involved (the procedure is non-trivial and is an active field of research!).
For the datasets 0 to 3, it can be said that, within uncertainty, the universes are open and will expand forever. Due to the physically anomalous nature of Data00, it's reasonable to conclude that the universe is flat as intended.
As to the remainder of the datasets (namely 4, 6, and 7), it is difficult to conclude with certainty as to whether they may correspond to open, flat or closed universes. In their current states, they're all approximately open although each are characterised by a time-varying dark energy component and so the flatness of each respective universe is subject to change in future time.

4 Conclusions

By analysing simulated data sets with respect to Friedmann's equation, the current best accepted parameters for our universe were further validated by a sort of process of elimination (whereby significantly different universe were seen not to be at all similar in expansion history or fit to our universe). In addition, when fit against accepted priors of approximate flatness and total matter density of $\Omega_m = 0.30 \pm 0.05$, the MCMC implementation produced cosmological parameters that fit the simulated supernova data extremely well.

Aside from the context of our universe, observing the behaviour of different cosmologies provided a more comprehensive look into the versatility and power of Friedmann's equation and MCMC as a method of curve-fitting a model to data. Cosmological parameters were fit to simulated supernova data that took into account even time-varying dark energy, and the produced fits

were all within an acceptable range of uncertainty with a high degree of statistical accuracy (the corresponding χ^2_{dof} values were never greater than 1.04). With these fits, it was found that most of the simulate data sets corresponded to closed universes that would continue to expand forever with the exception of one dataset which showed clear signs of eventual collapse due to positive curvature.

While analysing the data, several points of improvement were found that would be relevant for future studies. Firstly, Figures 7 and 16 were fundamentally limited in scope in that the curves were calculated according to scalefactor values and so the curve could not be calculated at points where the scalefactor was the same for two points in time (for example with recollapsing universes). This is a non-trivial task to rectify, and so would be a point of improvement in future papers. On top of this, the analysis was limited in that the mathematics of quintessence models are inherently more difficult to work with. A limitation due to this in this report is that there was no definite way to determine if a universe were to recollapse at some time once the dark energy lessened in expansion contribution. Furthermore, the time to collapse for quintessence models was incalculable under the time-frame in which this paper was written.

References

[1] Tamara Davis. "Cosmological constraints on dark energy". In: 2014. URL: https://arxiv.org/pdf/1404.7266.pdf.

[2] Tamara Davis. *Astrophysics III - Theoretical Notes*. 2022. URL: https://astrouq.github.io/PHYS3080_2022/TheoryCosmo.pdf.

[3] Tamara Davis. *PHYS3080 Cosmology Project Task Sheet*. 2022. URL: https://astrouq.github.io/PHYS3080_2022/CosmologyProject_2022.pdf.

[4] Randall Munroe. *Angular Diameter Turnaround*. 2022. URL: https://xkcd.com/2622/.

5 Appendices

5.1 Author Contributions

The main author (Ryan White) contributed all of the code for which the figures were produced and data analysis was performed. Some guidance was offered from the co-author Marin, particularly with respect to the horizon calculations in Figure 5.
This project would not have been possible without the programming framework and guidance supplied by Tamara Davis.

All programs, including the produced figures, and all data is available on the project's GitHub repository.

5.2 Supplementary Figures

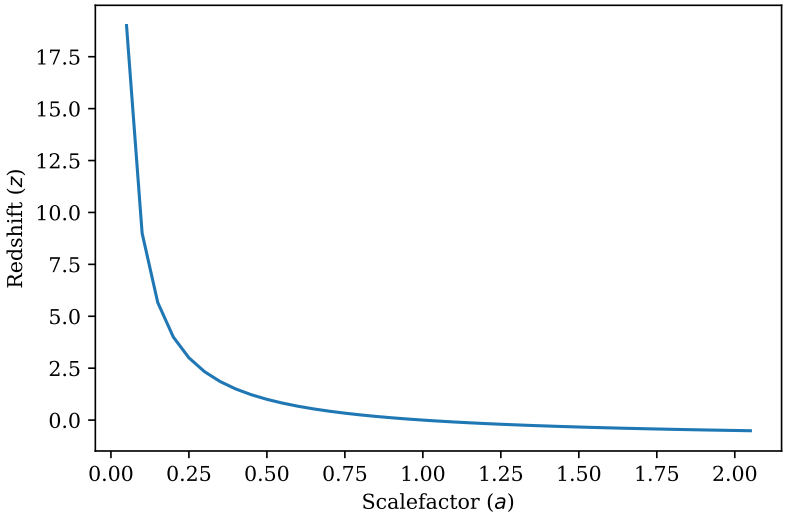

Figure. 17 As per equation (8), the observed cosmological redshift of a light source is inversely proportional to the scalefactor of the universe at the time of light emission. As such, looking at objects with higher redshift effectively corresponds to observing the universe at an earlier time, at least for objects of sufficiently high redshift. This relationship is independent of the cosmology of a particular universe.

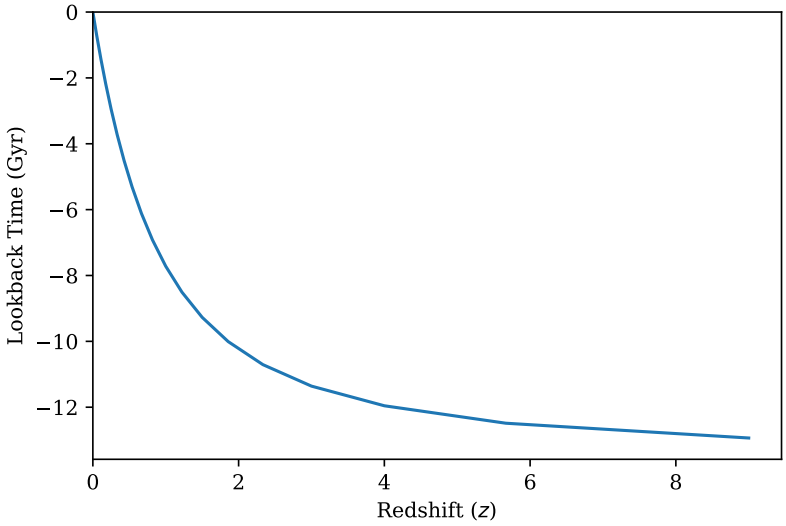

Figure. 18 As alluded to in the Introduction, observing light sources at higher cosmological redshift corresponds effectively to observing the universe at an earlier epoch. Represented here on the y-axis is the lookback time for our universe, which, as explained earlier, represents the time in relation to the present day $t = 0$.

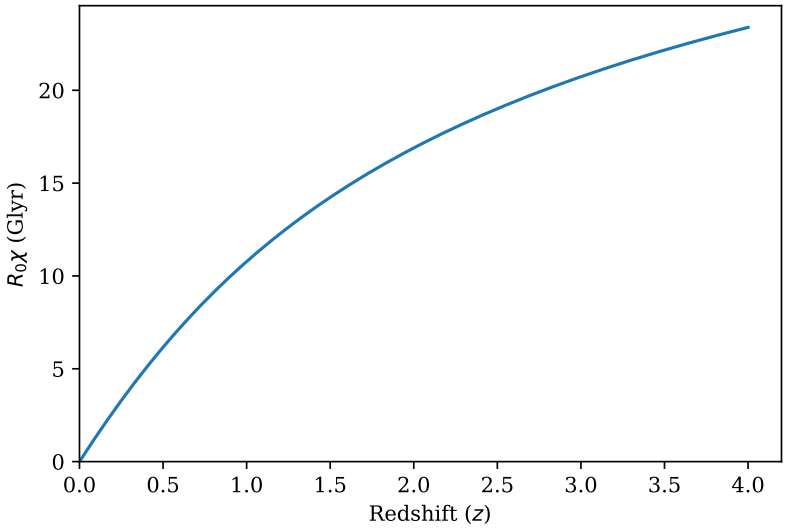

Figure. 19 Intended as a supplementary plot to Figure 5, this plot shows how comoving distance changes with redshift (and hence time). The code used to plot this graph was adapted to create the alternate x-axis (to show redshift) in Figure 5.

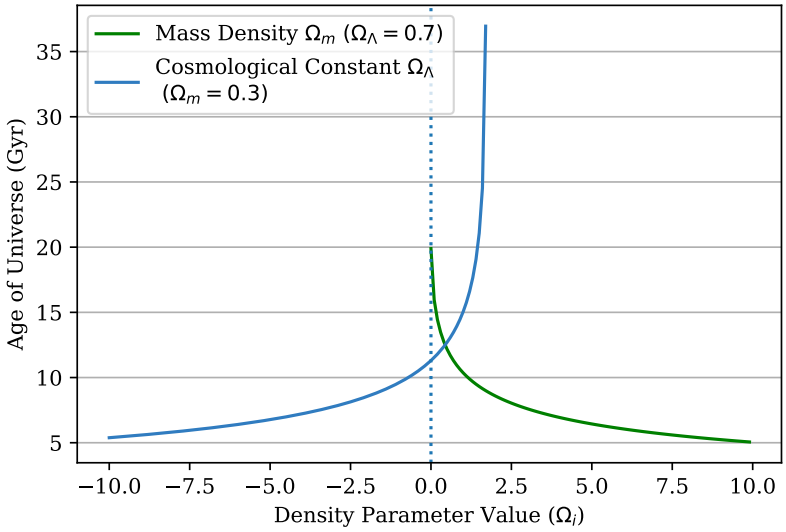

Figure. 20 As a companion figure to Figure 6, this plot shows the age of the universe with one cosmological parameter varying and the other fixed according the values in the legend. In agreement with Figure 6, this plot shows that for sufficiently high dark energy density that there is no big bang for a universe (age of the universe tends to infinity). The matter density curve is truncated at $\Omega_m = 0$ due to physical constraints.